Remote sensing of possible plasma density bubbles in the inner Jovian dayside magnetosphere

W. M. Farrell,[1] M. L. Kaiser,[1] W. S. Kurth,[2] M. D. Desch,[1] D. A. Gurnett,[2] G. B. Hospodarsky,[2] and R. J. MacDowall[1]

Received 10 July 2003; revised 22 December 2003; accepted 11 February 2004; published 22 July 2004.

[1] During the 2001 Cassini encounter with Jupiter, the Radio and Plasma Wave Science (RPWS) instrument detected fine spectral and temporal structure with broadband kilometric radiation. Applying known electron cyclotron harmonic radiation models, this microstructure is interpreted as originating from a plasma density depletion or bubble at the edge of the Io torus. The microstructure became very complicated at the event beginning and end (formation of broadband bursty structures), and this is interpreted as originating from high-frequency (3–4 s period) density waves or fingers found at the edge of the larger density bubble. Such high-frequency structure at the edges of plasma bubbles is reminiscent of small-scale structure associated with terrestrial spread-F density irregularities. We suggest that the narrow extended fingers, observed on a convex portion of the Io torus surface, result from the interchange instability that is shredding the outer edges of the plasma bubble. A similar set of circumstances occurring on a larger scale may explain the emission of Jovian radio bull's-eye emission observed previously by Ulysses. *INDEX TERMS:* 5737 Planetology: Fluid Planets: Magnetospheres (2756); 5719 Planetology: Fluid Planets: Interactions with particles and fields; 5780 Planetology: Fluid Planets: Tori and exospheres; 2756 Magnetospheric Physics: Planetary magnetospheres (5443, 5737, 6030); 2772 Magnetospheric Physics: Plasma waves and instabilities; *KEYWORDS:* Jupiter, Io torus, radio emission, electron cyclotron harmonics, interchange instability

Citation: Farrell, W. M., M. L. Kaiser, W. S. Kurth, M. D. Desch, D. A. Gurnett, G. B. Hospadarsky, and R. J. MacDowall (2004), Remote sensing of possible plasma density bubbles in the inner Jovian dayside magnetosphere, *J. Geophys. Res.*, *109*, A09S14, doi:10.1029/2003JA010130.

1. Introduction

[2] On 30 December 2000, the Cassini spacecraft made a distant encounter with Jupiter, passing to 137 R_J of the planet and entering, for two short periods, into the planetary magnetosphere [*Kurth et al.*, 2002; *Gurnett et al.*, 2002]. During the inbound period, Cassini's Radio and Plasma Wave Science (RPWS) instrument observed a most interesting broadband kilometric (bKOM) radio emission from the frontside magnetosphere that at times exhibited very complicated spectral microstructure. *Kurth et al.* [2001] first reported this interesting microstructure, suggesting it resulted from either a fringe propagation effect or fast-variation source phenomenon. This report discusses these observations in detail and attempts to model the emission source character based on its newly observed microstructure.

[3] Broadband kilometric emission was first observed with relatively low spectral (many kHz) and temporal (seconds) resolution with the Voyager Planetary Radio Astronomy (PRA) and Plasma Wave (PWS) experiments [see *Carr et al.*, 1983, and references therein] and later with the Ulysses Unified Radio and Plasma Wave (URAP) instrument [*Kaiser et al.*, 1992; *Stone et al.*, 1992] and Galileo PWS [*Kurth et al.*, 1997]. The current observations feature the Cassini RPWS system consisting of five radio receivers, a sounder and Langmuir probe providing enhanced spectral and temporal coverage and resolution [*Gurnett et al.*, 2004]. When bKOM is examined using Cassini's low-resolution High-Frequency Receiver (HFR), the emission appears relatively smooth in both frequency and time. However, when examined with high-resolution waveform (wideband receiver (WBR)) measurements, complicated narrow and broadbanded microstructure is revealed for the first time within the event [*Kurth et al.*, 2001].

[4] Figure 1a shows an occurrence of bKOM emission observed between 0230 and 0320 spacecraft event time (SCET) on 21 October 2000 from *Kurth et al.* [2001]. As observed in the HFR receiver (Figure 1a), the emission appears very similar to the bKOM emission reported previously during the Voyagers and Ulysses frontside inbound approaches to Jupiter: a broadband emission between 20 and 100 kHz, with quick frequency drifts upward and downward on the order of minutes [*Warwick et al.*, 1979]. Voyager observations [*Kurth et al.*, 1980] suggest that the events are observed typically when the spacecraft extends to higher magnetic latitude, with a distinct "shadow zone"

[1]NASA Goddard Space Flight Center, Greenbelt, Maryland, USA.
[2]Department of Physics and Astronomy, University of Iowa, Iowa City, Iowa, USA.

0148-0227/04/2003JA010130$09.00

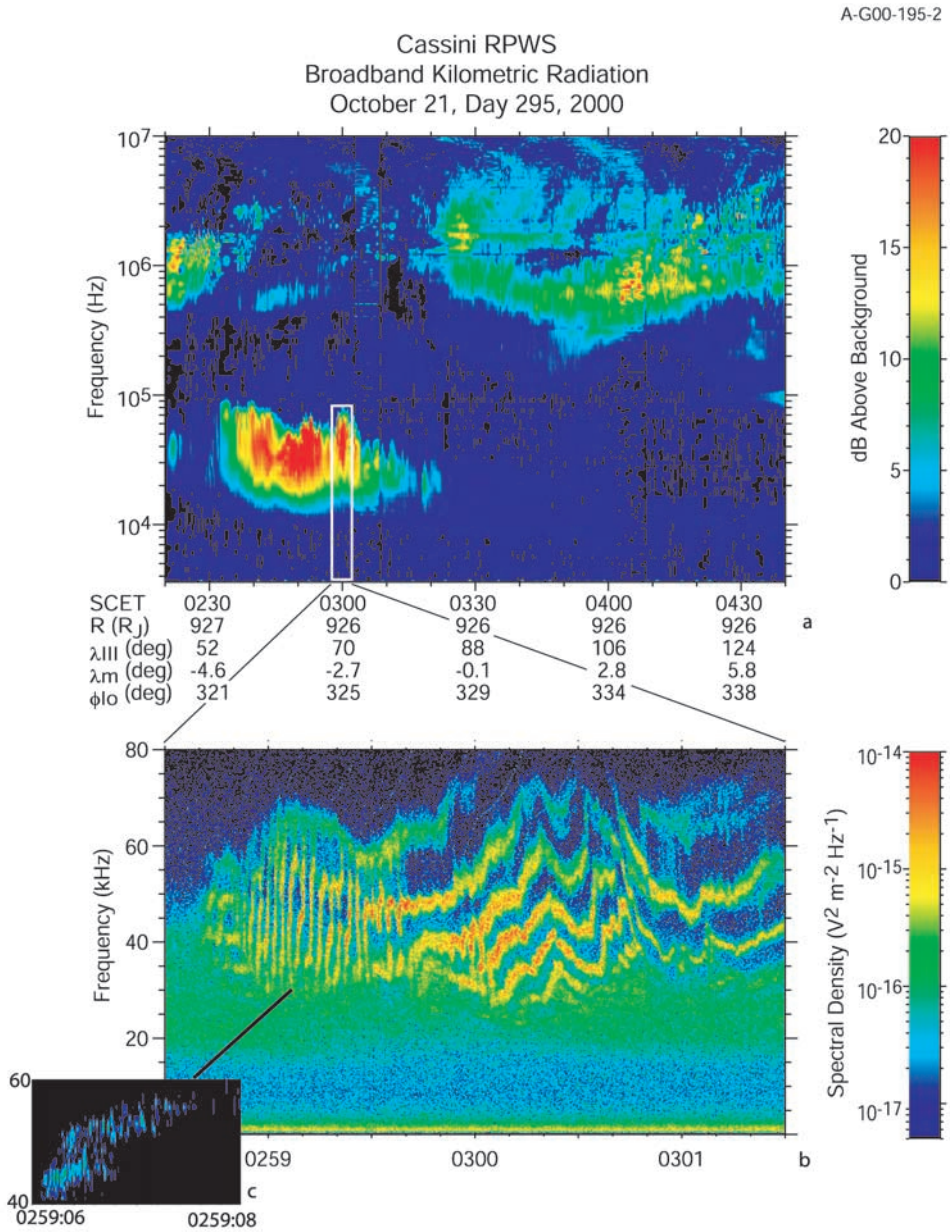

Figure 1. A broadband kilometric radiation event as observed in the Cassini Radio and Plasma Wave Science (RPWS) (a) High-Frequency Receiver (HFR) with broad spectral and temporal resolution and (b) the wideband waveform receiver with enhanced spectral and temporal resolution. Note that the initially amorphous emission contains detailed microstructure, with bursty emissions before 0259:30 SCET evolving into narrow tones. Bursty events appear again near 0301:00 spacecraft event time (SCET). The inset (Figure 1c) shows a very high resolution waveform image of an individual broadband burst indicating its composition consisting of a set of updrifting narrow tones.

found at equatorial latitudes associated with source occultation from the Io torus. However, Ulysses found that isolated solar wind density structures associated with corotating streams and shocks had a profound effect on bKOM, escaping continuum, and quasi-periodic (QP15)- bursts, effectively turning on all their Jovian radio sources quasi-independent of spacecraft/torus positioning for days immediately following a shock's or corotating stream's collision with the planet [*Kaiser et al.*, 1992]. In fact, during these solar wind driven periods, bKOM, continuum, and QP emissions tended to blend together making a differentiation of components difficult. It has been argued that QP bursts and escaping continuum may actually merge at low frequencies into a single escaping component [*Kaiser*, 1998]. During the observation period presented in Figure 1, Cassini was inbound to Jupiter at ~10.7 hours LT, at $-3°$ magnetic latitude and about 926 R_J from the planet.

[5] Unlike the two Voyagers and Ulysses, the Cassini RPWS has a wideband receiver (WBR) capable of sampling signals from various antennae at 222 kS/s, thus allowing

high-resolution waveform measurements in a continuous band pass up to near 80 kHz. Fortuitously, the WBR obtained a high-resolution snapshot during the latter part of the bKOM event in Figure 1a, between 0256 and 0302 SCET. This high-resolution spectrogram is shown in Figure 1b. The microstructure observed between 0300 and 0302 SCET consists primarily as a set of drifting narrowband tones each separated by 10–15 kHz. Such tones have been observed from both terrestrial and Jovian magnetospheres (i.e., myriametric or continuum emissions) in association with electron cyclotron harmonic radiation from sharp plasma density boundaries (i.e, terrestrial plasmapause, Io torus) [*Gurnett*, 1975; *Jones et al.*, 1976; *Jones and Leblanc*, 1987; *Kurth et al.*, 1981]. However, for the earlier period between 0258:30 and 0259:30 SCET, the emission is unusually complicated with the appearance of quasi-periodic broadband bursty emissions of >30 kHz bandwidth. These bursts reoccur with ~3–4 s repetition. The narrowband tones seen later appear to be completely absent during this early time.

[6] A critical observation is the transition period from 0259:30 to 0259:45 SCET. For this 1/4-min interval the broadband burst structure fragments into a set of narrow tones that possess highly fluctuating center frequencies. The narrow tones are ~2 kHz wide but their center frequencies quickly upshift and downshift by ~10 kHz on time scales of seconds, at times slurring the set of narrow tones into a broader-band emission (appearing like a remnant broadband burst). This revealing period suggests the broadband bursts observed before 0259:30 SCET are not intrinsically broadbanded but instead consists of a set of intrinsically narrow tones undergoing a quick frequency shift and hence the appearance of a merged broadband emission. To check this, the single broadband burst at 0259:06–0259:08 SCET was examined with high time resolution fast Fourier transform (FFT) analysis, shown in Figure 1c, with a factor of 16 times smaller time window than that used in Figure 1b. Note that at high resolution, the original broadband burst does indeed consist of two narrowbanded updrifting tones undergoing a 7–10 kHz frequency up-drift on the order of 1 s. As we discuss below, this observation suggests the narrowband source location is undergoing a strong physical variation.

[7] After 0259:45 SCET, the quick variations in the narrow tone's center frequencies stabilize, smoothly evolving into a set of steady slow-drifting narrow tones (of ~2 kHz bandwidth each) that are observed from 0259:45 to 0301:30 SCET. We note that weaker broadband bursty events are again observed from 0301:30 to 0302:00 SCET near the end of the event.

[8] In this work we attempt to interpret this complicated structure as a phenomenon associated with the radio source (and assume propagation effects are minimal). We apply known radiation generation models of myriametric emission and, in essence, invert these to infer the changing magnetospheric configuration at the radio source in the inner Jovian magnetosphere. We assume that the emission propagates from its magnetospheric source to the spacecraft freely, at frequencies well above the magnetosheath nose plasma frequency. We ultimately surmise that the emission is generated by a sharp density hole at the edge of the Io torus, which gives rise to the overall drifting of the narrow tones. The observed broadband structure found preceding and following the event is interpreted as originating from a set of regularly spaced thin density extensions or fingers occurring at the edge of the bubble.

2. Myriametric Radiation Models

[9] It has long been recognized that the source of terrestrial myriametric emission occurs at steep density gradients associated with magnetospheric boundaries [*Gurnett*, 1975; *Kurth et al.*, 1981]. *Jones* [1976] suggested that intense electrostatic emissions on the high-density (plasmasphere) side of the boundary, like the $(n + 1/2)\, f_c$ emission, linearly convert to the freely propagating o-mode electromagnetic branch on the low-density (magnetosphere) side of the boundary via a wave-wave radio window (linear mode conversion). In this case the strongest electromagnetic emission is generated for the $(n + 1/2)\, f_c$ electrostatic emission nearest the local plasma frequency at the boundary. *Jones* [1986] and *Jones and LeBlanc* [1987] explicitly suggested this mechanism to explain Jovian kilometric radiation which was suspected to originate from the outer Io torus. Conversely, it has recently been suggested [*Farrell*, 2001] that energetic electrons at a gradient boundary can emit o-mode emission by direct coupling of their free energy to those electron cyclotron harmonic emissions at frequencies above the local plasma frequency via relativistic electron cyclotron harmonic resonance. Calculations indicate that the wave phase velocity resonance ellipse [*Wu and Lee*, 1979; *Omidi et al.*, 1984] converges to low parallel and perpendicular velocity values near $f \sim nf_c$ and f_p, ($X = f_p^2/f^2 \sim 1$ and $Y_n = nf_c/f \sim 1$) making possible wave interaction with low-energy electrons via the cyclotron harmonic resonance. Appendix A summarizes the resonant interaction via the electron cyclotron harmonic (ECH) maser model.

[10] While the two mechanisms differ in detail (wave-wave versus wave-particle interactions), their primary manifestation is the same: Given a steep density gradient (a quickly decreasing plasma frequency) at a boundary (Figure 2a), a set of narrowband o-mode emissions will be generated as the local plasma frequency sweep through the various $(n + 1/2)f_c$ bands (for the Jones model) or $\sim nf_c$ harmonics (for the ECH maser model [*Farrell*, 2001]). In either case, a set of narrowband tones are generated, each separated by the local electron cyclotron frequency at the boundary. The two models differ only in that the tones will be shifted by a constant $f_c/2$, depending upon the model selected. An example spectrogram of this conversion at the terrestrial plasmapause boundary is shown in Figure 3, with upper hybrid emissions near the local plasma frequency on the high-density (right-hand) side and radiating narrowband o-mode emission on the low-density (left-hand) side of the boundary. The Jones model would suggest that the $f_{uh} \sim (n + 1/2)\, f_c$ emissions linearly convert to o-mode bands, with f_{uh} being the upper hybrid frequency. The electron cyclotron harmonic maser model [*Farrell*, 2001] would suggest that the same energetic, anisotropic electron distributions responsible for the electrostatic emissions [see *Kurth et al.*, 1979, Figure 3] are also the free energy source for the freely propagating o-mode bands via the relativistic cyclotron harmonic resonance.

[11] For radiation at frequencies below the magnetopause plasma frequency, these narrow o-mode emissions are

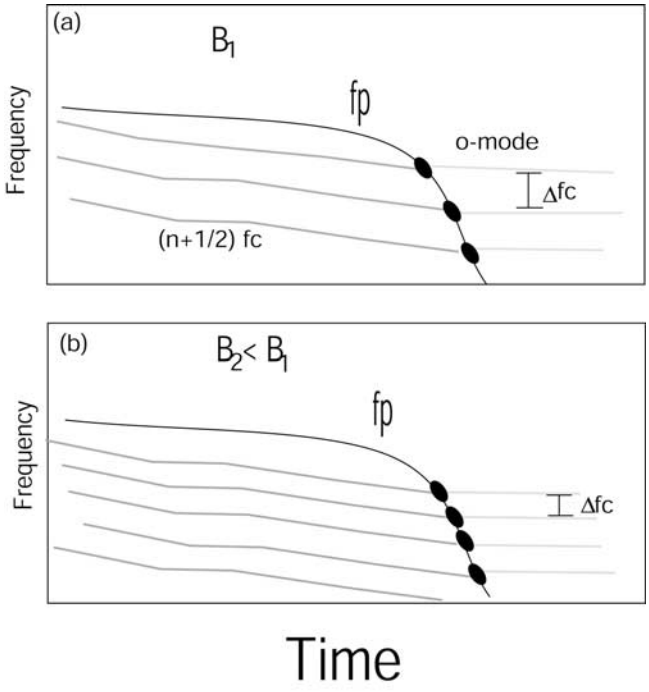

Figure 2. An illustration of a spectrogram from a spacecraft crossing a density gradient. Note that as the plasma frequency passes by each cyclotron harmonic, escaping emission can be generated either via linear mode conversion [*Jones*, 1976] or direct wave/electron coupling [*Farrell*, 2001]. As field strength decreases, the frequency interval between modes decreases. Narrowband emission is generated from this process.

considered trapped, reflecting from the magnetosphere cavity walls, essentially giving rise to Doppler broadening of the tones into a true spectral continuum [*Barbosa*, 1981]. However, for emissions at frequencies well above the magnetopause plasma frequency, the narrow tones from the boundaries freely escape the magnetosphere and can be detected by spacecraft at large distances from the planet [*Gurnett*, 1975].

[12] As suggested by Figure 2, the spacing of the radiated tones will differ given similar steep plasma density gradients at two different magnetospheric locations having different ambient magnetic field strengths, B_1 and B_2. Assuming the magnetic field is quasi-rigid in the inner Jovian magnetosphere, the harmonic radiation from the plasma gradients becomes a telltale signature of the gradient's radial location. Further, assuming a corotating radiation source, the variation of the harmonic emission with time as viewed from a distant observation point (i.e., Cassini) reveals the gradient's azimuthal structure.

3. Model Application

[13] *Jones* [1986] and *Jones and LeBlanc* [1987] suggested explicitly that the linear conversion theory applied directly to Jovian kilometric radiation, and *Farrell* [2001] suggested that the ECH maser model may be applicable to the analogous terrestrial continuum radiation. We now apply these density gradient/electron cyclotron harmonic models to the observations in Figure 1b and 1c. In the application we make the following assumptions: First, that the emissions are functionally-related to electron cyclotron harmonics originating from a steeply decreasing, quasi-radially directed plasma density gradient $-\nabla \mathbf{n} \sim -\nabla n(r_o + \delta r, \varphi_o + \delta\varphi)\mathbf{r}/|\mathbf{r}|$, where $\delta r/r_o \ll 1$ and $\delta\varphi/\varphi \ll 1$ and $\mathbf{r}/|\mathbf{r}|$ is the radial unit vector. Given the kilometric emission bandwidth from 25 to 100 kHz in Figure 1a, we infer that the density gradient varies from 3 to 125 el/cc in a spatially localized region. Second, that the variation in the cyclotron harmonic structure is associated with the radial location of the gradient in the Jovian planetary magnetic field. Basically, as the set of cyclotron harmonics drift to higher frequencies, we infer that the gradient has extended closer to the planet where the magnetic field strengths are greater. As the set of harmonics drift to lower frequencies, we infer that the gradient has extended outward into regions of weaker magnetic fields. Finally, we assume the source is corotating and that the emitted rays follow a direct radial path from a gradient with a quasi-radial normal to the spacecraft. In essence, these assumptions imply that the observations in Figure 1b represent the radial variations of a longitudinally

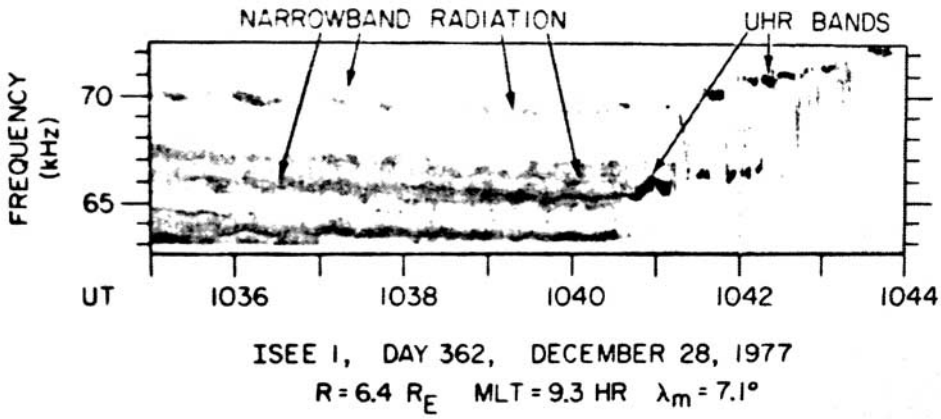

Figure 3. The generation of radiated narrowband tones at the terrestrial plasmapause [*Kurth et al.*, 1981]. Emissions are generated at electron cyclotron harmonics near the local upper hybrid (UHR) frequencies. In this plasma, $f_{uhr} \sim f_p$.

extended density gradient. As the structure corotates, Cassini is viewing emissions from a portion of the radially varying gradient in direct view.

[14] Before exploring the details of the gradient structure, we will make some broader applications of the above model. First, near 0300 SCET, the presumed cyclotron harmonics are separated by a cyclotron frequency, fc ~12 kHz, which places the gradient near 9–10 R_J. This location is consistent with being at the outer edge of the Io torus [*Bagenal*, 1994; *Kurth et al.*, 2001], where density variations are anticipated. Second, assuming corotation, the entire structure appears to be about 2–3° in azimuthal extent and thus is relatively small compared to the entire 2π torus. Finally, we note that emission has a distinct spectral signature from 0259 to 0302 SCET but from 0256 to 0259 SCET appears as a quasi-diffuse continuum. We infer that the steep density gradient is not omnipresent along the torus but instead is localized.

[15] In order to derive the detailed radial/longitude gradient position, $\nabla n(r_o, \varphi_o)$, we select the fourth harmonic (that visible throughout the entire event) and follow its progression in frequency and time. In essence, the frequency relates to the radial position via

$$f = n\, f_c = n\, 2800\, M/r^3, \quad (1)$$

where f is in kHz, n is the harmonic number, M is the planetary magnetic field dipole moment of 4.3 G R_J^3, and r is scaled to the planetary radius. For the fourth harmonic,

$$r = 36.2 f^{-0.333}. \quad (2)$$

Assuming corotation, time relates to longitude via

$$\Delta\varphi = 360^\circ \delta t/T, \quad (3)$$

where δt is the relative time of the emission and T is the planetary rotation period of 9.92 hours (595.2 min). This corotation corresponds to ~0.6° per min. The transformations in equations (2) and (3) allow the conversion from the frequency/time structure of the fourth harmonic to the gradient's radial/azimuthal location. The results are illustrated in Figure 4.

[16] Note from Figure 4 that the overall structure is associated with a density "biteout" or depression in the outer Io torus, with the gradient location making an inward radial excursion from ~10.1 R_J to ~8.6 R_J. This density depression is about 1.2° wide. The bursty variations in the emission observed at the beginning and end of the event are interpreted as coming from a series of very narrow density structures (regularly spaced density "fingers" or density waves) at the edges of the overall larger depression. The structures have large radial extents (~1 R_J) but occur in azimuthally localized regions (~0.05° or ~500 km width), leading to large frequency excursions of each of the harmonics in a relatively short time period (i.e., resulting in apparent broadband bursts). For example, near 0259:35 SCET the center frequency of the fourth harmonic quickly upshifts from 42 to 50 kHz, and application of equation (1) indicated this shift is in association with a steep spatial variation in radial position of the density gradient from 9.8 to 10.4 R_J. This radial change occurs in a very limited longitudinal region, which via corotation, corresponds to short time scales (the wideband FFT processing window for Figure 1b), thus producing the frequency-extended, near-vertical updrifitng tone on the spectrogram. Simultaneously, the third harmonic shows a similar quick updrift from 32 to 41 kHz. Together these two broad harmonics form almost a complete merged broadband bursty event, with only a small frequency gap near 41 kHz allowing some distinguishing between the two bands. In situations where there are larger radial excursions on shorter time scales, overlapping, indistinguishable bands will develop in Figure 1b, these forming complete broadband bursts like those observed near 0259:00 SCET. As indicated in Figure 1c, a high-resolution image of these broadband bursts reveals their underlying drifting narrowbanded nature consistent with the idea that the emission is intrinsically narrowbanded but from a source undergoing a large radial variation in a very limited azimuthal angle. This process "blends" (more like "smears") the drifting narrow tones (~10 kHz drift in 1 s) into a broadband structure when viewed at intermediate time scales (~3 min). Appendix B demonstrates the development of this structure in detail via radiation model analysis.

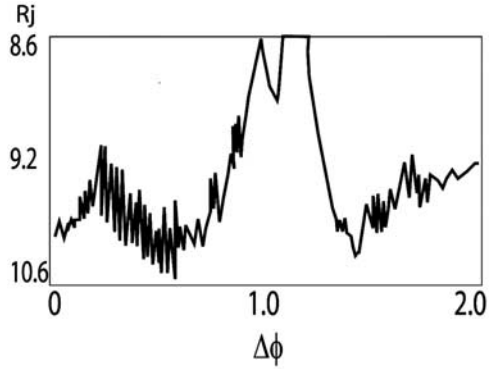

Figure 4. An illustration representing the location of the sharp density gradient responsible for the electron cyclotron harmonic (ECH) emissions observed by Cassini RPWS (Figure 1b). Note that small-scale density variations lie on either side of the primary depletion.

[17] Equation (1) above assumes that emission is generated at the local harmonic and not the 1/2-harmonic frequency. If the latter assumption is applied, the frequency coefficient in equation (1) is modified by $(n/(n + 1/2))^{1/3}$. Since the modification has an effect to the 1/3 power, a shift of fourth harmonic to its half counterparts ((n + 1/2) f_c, n = 3, 4) results in only a 4% difference in calculated radial position. Thus the assumed model n versus n + 1/2 affects the results only in a minor way and the illustrated profile in Figure 4 is approximately correct for either model.

4. Interpretation

[18] Using density-gradient/cyclotron harmonic emission models [*Jones*, 1976; *Farrell*, 2001], we interpret the kilometric emission microstructure as being emitted from a density biteout at the outer edge of the Io torus. This depression extends about 1–2° in azimuth. Most interesting is the observation of higher-frequency density waves or

fingers located about the edges of the larger depression. Between 0258:30 and 0259:30 SCET, these fast, very regular fingers have a period of about 3–4 s.

[19] We consider two possibilities for the formation of the fingers. First, such high-frequency activity is expected at the edges of a large MHD structures as a natural consequence of dispersion. As described by *Tidman and Krall* [1971], all available plasma modes from low to high frequencies are involved in creating a structure with a distinct and well-defined boundary (i.e., all modes are required to make a step function). Typically, in a dispersive medium, high-frequency modes have larger propagation velocities and thus after a period of time will tend to propagate ahead of the primary structure. In the case of MHD shocks, high-frequency whistlers initially required to make a distinct step-like shock boundary will propagate ahead of the Alfvenic shock [*Tidman and Krall*, 1971]. The shock will lose some of its high-frequency character in the process (rounded edges, reduced slope).

[20] A similar basic plasma physics phenomenon might be occurring at this torus density bubble. Initially, the bubble was a distinct sharp MHD structure, but as the structure evolved in time, the higher-frequency wave modes required to make the structure "distinct" propagated into adjacent regions, thus giving rise to the high-frequency structures observed adjacent to the primary structure. In the process, the edges of the primary density biteout became more gradual, in essence "dissipating" the structures high-frequency energy.

[21] An analogy is the terrestrial ionospheric spread-F phenomenon detected by HF radar [*Basu et al.*, 1986], in situ rockets [*Kelley et al.*, 1986] and low-orbiting spacecraft [*Aggson et al.*, 1993]. Large-scale ionosphere density bubbles develop due to the Raleigh-Taylor fluid instability, ranging from hundreds of kilometers in height and tens of kilometers in width. However, observation [*LaBelle and Kelley*, 1986] and simulation [*Zalesak et al.*, 1982] indicates that secondary small-scale modes about the bubble perimeter are also excited, these with scale sizes from 1 km to a few meters. The small-scale modes are the actual reflection sites for the HF radar signals. Simulations of *Zalesak et al.* [1982] indicate that the relative motion of the bubble and surrounding plasma will create locations along the bubble perimeter with highly compressed electron density gradients. These sharp gradient regions tend to be unstable to the smaller-scale wave modes via density gradient or

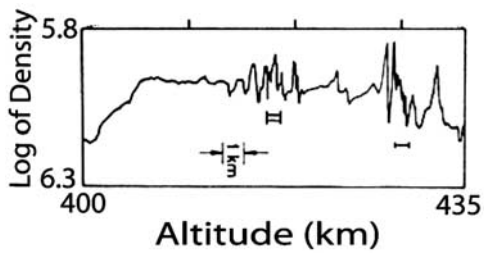

Figure 5. Ionospheric density from the Condor rocket flight showing a 30 km spread-F plasma bubble and associated intermediate-scale structure on the high-altitude bubble top (Region I activity). Figure adapted from *Labelle and Kelley* [1986].

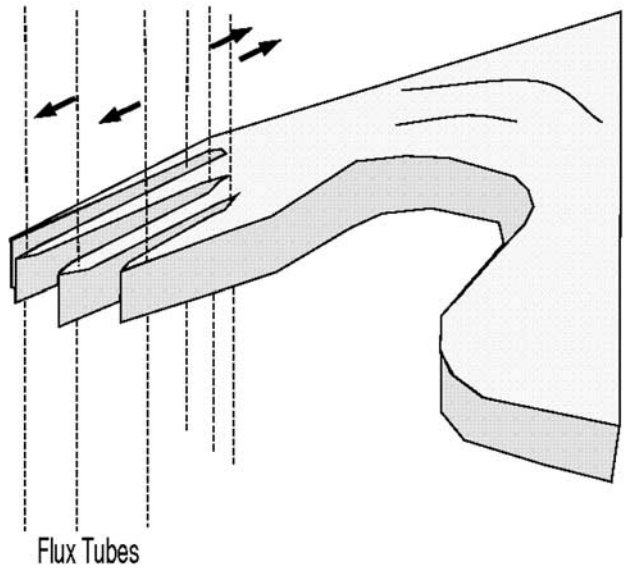

Figure 6. Flux tube movement and extension of torus undergoing interchange instability.

gravitational drift modes. In essence, where the boundary becomes too sharp, natural processes occur to smooth it out. Figure 5 (adapted from *LaBelle and Kelley* [1986]) shows a spread-F bubble observed during the upleg portion of a rocket flight. The intermediate scale turbulence at the bubble top is associated with a topside boundary instability, giving rise to secondary fluctuations superimposed on the larger fluid instability. Thus turbulence at bubble edges is an expected phenomenon as the exterior plasma tries to erode sharp spatial edges into a smoother surface.

[22] A second, related possibility for the high-frequency finger formations involves the interchange instability, which is known to operate along the torus edges [*Yang et al.*, 1992, 1994]. In this case we consider its operation on microscopic scales. Specifically, the outer edges of the density bubble have convex-shaped surfaces while the inner bubble structure itself is concave (see Figure 6). The former geometry tends to be unstable to the interchange instability while the latter is stable. As such, we could interpret the high-frequency oscillations at 3 s scales along the convex portion of the surface as resulting from the interchange instability acting on azimuthal scales of $\sim$0.03° ($\sim$350 km separation). In order to account for the slurring of the harmonics into a broadband pulse, the radial dimensions of the instability's finger-like structures appear to extend on the order of a planetary radii. In essence, the wave emission indicates this convex portion of the torus is in the process of being "shredded" by the exterior plasma via the interchange process.

[23] As described by *Yang et al.* [1994], the growth criteria for the interchange instability involves the competition between the cold and energetic plasma components. The former has a decreasing density with increasing radial distance at the torus edge and thus is inherently unstable to the interchange process. In contrast, the latter has increasing density with increasing radial distance at the torus edge, which provides stability that can offset the unstable contribution from the cold component. As described by *Yang et*

al. [1994, equation (15c)], a single torus edge can become unstable in regions where there is an unusually steep negative gradient in cold plasma density per unit magnetic flux. This condition for the interchange instability is perfectly consistent with the radiation model presented here that also requires a steep negative density gradient, $\delta r_o/r_o \ll 1$. Hence a steep gradient, the interchange instability, and well-defined cyclotron harmonic radiation may be all systemic processes.

[24] There are three pieces of evidence that weigh in favor of a microscopic interchange process. First, the finger structures at the edges are quasi-monochromatic (inferred from the regularly spaced broadband pulses). The regularity suggests the presence of a monochromatic fluid wave at the boundary that is expected during the early (linear) portion of an instability. In fact, if the density structures on the bubble's edges were more turbulent (irregular shaped and spaced), the density r/δ positioning would be quasi-random, giving rise to a diffuse ECH emission structure. The presence of regularly spaced broadband pulses observed at ~3 s intervals suggests the presence of a set of well formed but longitudinally thin density structures with distinct and sharp density boundaries. Second, as inferred from the detailed evolution from narrow to broadband emission, in order to account for the cyclotron emission structure, the evolution of the finger structures along the convex portion of the surface starts out with small structures at the inner edge of the density bite out that eventually become larger in the more convex portion of the density wall (see Figure B3). This evolution would be anticipated for a growing MHD wave mode. The mode appears to grow to full strength (tones go from stable narrowband to broadbanded) in about 30 s or 0.3° in longitude (corresponding to 0.05 R_J). The mode itself has a 0.03° periodicity (or ~350 km wavelength), suggesting the instability becomes fully activated in about 10 wave cycles. This sort of mode evolution is typical for an unimpeded plasma instability. Third and foremost, the instability appears to cease in the concave portion of the boundary, consistent with the interchange process. From 0259:45 to 0301:00 SCET, when the gradient location extends inward, there is almost a complete cessation of high frequency fluctuations, with narrow steady tones observed throughout this concave portion of the bubble. After 0301:00 SCET, a weaker, less defined set of broadband bursts are again observed adjacent to the bubble, suggesting small density finger formation in an apparent convex portion of the boundary.

[25] It may seem unusual that the fingers have large radial extents relative to their azimuthal dimensions, with the ratio of length to width approaching a factor of 100. However, we note that terrestrial ionospheric spread-F also creates long fingers with length-to-width ratios near a factor of 20 [*Zalesak et al.*, 1982]. Thus the formation of extended but still coherent structures is possible, we suspect, primarily during the early stages of the MHD instability.

5. Nature of Jovian Kilometric Radiation: Source Location and Manifestations

[26] The source of Jovian kilometric emission is the subject of some debate. Specifically, models of *Jones* [1986] and *Jones and Leblanc* [1987] rely on a source in the outer flanks of the torus. Conversely, *Green and Gurnett* [1980] and *Ladreiter et al.* [1994] present the possibility that emission originates from the high-latitude footprint from magnetic field lines threading the Io torus. The latter performed their analysis assuming emission is generated near the shell of constant cyclotron frequency near 100 kHz.

[27] Cassini's direction-of-arrival system is designed to determine emission source location to about 1° accuracy. Consequently, the event in Figure 1, detected at about 1000 R_J, could be localized to no better than 20 R_J which is too broad to be of real use in this work. However, some inferences on the location can be obtained from the emission phenomenology. Specifically, the particular bKOM event shown in Figure 1 consists of an hour long episode with emission detected below 30 kHz observed by Cassini when it passed from −5° to −0.3° [*Kurth et al.*, 2001]. This event occurrence does not show evidence for a "shadow zone" effect at equatorial latitudes as would be expected from an auroral emission. Significantly, for an electron cyclotron fundamental source at or below 30 kHz, the shell of constant cyclotron frequency that is contained in the magnetosphere (on closed field lines, $L < 15$) is that portion extending from ±30° magnetic latitude out near 7–8 R_J (see the 1000 nT contour in Figures 1.23 and 1.24 of *Acuna et al.* [1983]). In essence, one cannot consider this a "high-latitude" auroral source in the same context as auroral kilometric radiation, Saturn's kilometric radiation, etc. The viable magnetospheric sources <30 kHz all lie at large radial distances out at the quasi-equatorial edges of closed field lines. These field lines thread right through the outer edge of the torus, in a location where f_p is comparable to f_c. Finally, even though the emission energy is derived from cyclotron emission (either the $(n + 1/2)\ f_c$ or nf_c harmonics), the emission microstructure fast fluctuations suggests that the local plasma frequency has a strong controlling effect (e.g., Figure 2). Thus the extreme variability of the source as seen in the emission microstructure is consistent with changes in the local plasma frequency, placing the source at/near the torus where f_p is comparable to f_c.

[28] We suggest that a number of low-frequency emissions (<100 kHz) previously considered independent components, like those called "narrow tones" [*Gurnett et al.*, 1983], low-frequency broadband kilometric radiation (bKOM) [*Warwick et al.*, 1979], and Jovian bull's-eyes [*Kaiser and MacDowall*, 1998] really come from the same source, the torus, but under differing torus conditions. Specifically, *Kurth et al.* [2001] show numerous examples of high-resolution narrow tones as part of bKOM, and we have interpreted those narrow tones as coming from a steep density gradient at the torus edge. If the gradient changes position under the influence of a larger instability, the tones will drift (either slowly or quickly) and even form broadband structures. As discussed in Appendix C, the Jovian bull's-eyes detected by Ulysses could also be explained as ECH emission from a torus undergoing a large interchange instability process like that envisioned by *Yang et al.* [1992, 1994]. Finally, when kilometric emission appears diffuse, the torus edge is considered to have numerous random modes, resulting in a randomized gradient location and ECH emission at all frequencies. Thus rather than considering these different components as separate, we might label them all as torus kilometric emission (t-KOM), and consider

the change in features as differing manifestations of the same torus source. As decribed by *Kaiser and MacDowall* [1998], Jupiter contains a ''zoo'' of radio emissions, approaching over nine separate components. However, we suggest here that three or possibly four components may actually be from the same source and generated via the same process, just appearing different because the source itself has a different manifestation.

[29] It should be noted that this t-KOM thought is not really new but an implicit theme in the series of Jones papers from 1976 to 1987. The current work really only applies these thoughts to the new Cassini wideband events and Ulysses bull's-eyes, further confirming Jones' overall theme of the torus as the source of low-frequency kilometric radiation. In fact, given the nature of the early Jovian data sets, which where primarily low resolution measurements, Jones' theme was rather forward thinking.

6. Conclusion

[30] Using the high-resolution capability of the Cassini RPWS, we suggest that the VLF emission microstructure associated with a portion of a bKOM event is a result of electron cyclotron harmonic-related emission from a density bubble in the outer Io torus. Associated broadband bursty emissions observed both preceding and following the primary structure are interpreted as resulting from an interchange instability from the intrinsically unstable convex portion of the steep torus boundary.

[31] In order to derive these results, we assume the radio source is a sharp, distinct, quasi-radially directed density gradient like that associated with the terrestrial plasmasphere. We further assume that electron cyclotron harmonic (or 1/2 harmonic) emissions are generated from said gradient and their spacing is indicative of the radial location of the gradient via equation (1). Finally, we assume the entire plasma structure corotates thereby allowing a view of the source at progressively changing longitudes as described by equation (2). We implicitly assume that the density varies against a background quasi-rigid magnetic field. While the interchange process itself suggests B is nonrigid, we assume that interchange perturbations to B are small and do not effect the emission process. The density variation/gradient movement accounts for the tonal variations. Our interpretation is dependent on these assumptions and changes in one or all of these assumptions will give rise to a new interpretation. Consequently, the model is not unique, and other interpretations are possible. However, we are applying well-known emission mechanisms [*Jones*, 1976; *Jones and Leblanc*, 1987; *Kurth et al.*, 1981] to the events in Figure 1, and while not truly unique, there is a strong likelihood that this scenario is possible, given the ubiquitous previous observations of electron cyclotron harmonic-related emission from the terrestrial plasmapause and Io torus.

[32] Observational evidence that the torus undergoes large-scale fluid instabilities featuring density variations on a quasi-rigid magnetic field was found during the 1992 Ulysses/Jupiter encounter. During the encounter, the spacecraft passed from northern to southern latitudes near 6 R_J at the same time the centrifugal equator (containing the torus) also swung downward. The end result of this fortuitous geometry was that Ulysses maintained a quasi-constant magnetic latitude ($\sim$30°N) and radial distance over the torus top for nearly 1/2 a planetary rotation. During this time, the Ulysses URAP instrument monitored the local plasma frequency as the torus quickly passed beneath it and found that the torus possessed a set of intense density depletions [*Farrell et al.*, 1993] spaced approximately 17° apart in longitude [*Desch et al.*, 1994]. Their spacing is consistent with the *Yang et al.* [1992, 1994] MHD model of a torus undergoing a large-scale interchange instability. While these Ulysses measurements suggest a much larger macroinstability associated with the torus, fluctuations in the plasma frequency ($\sim$30% changes in density) were observed down to the 144 s ($\sim$1.5°) resolution of the measurement. The high-resolution measurements presented here suggests the fast density fluctuations can occur at even smaller scale, down to a few seconds, as suggested by Figure 1b.

[33] There is some parallel of narrow tones of t-KOM discussed here to terrestrial ''kilometric continuum'' recently reported by Image/RPI investigators [*Green et al.*, 2002]. Specifically, terrestrial kilometric continuum appears as a set of banded emission and is suspected of being generated from significant density depressions in the terrestrial plasmapause. These sharp, well-defined density cavities (or density canyons) are filled with escaping harmonic emission. Similar density depressions filled with emission have also been observed from the canyon-like density cavities of the Io torus [*Farrell et al.*, 1999]. Based on the analogy to Jovian emissions, terrestrial kilometric continuum might be consistently used as a remote-sensing diagnostic of plasmapause conditions.

[34] *Kurth et al.* [2001] suggested the broadband emissions might be generated by a source phenomenon (violent fluctuation) or a possible interference fringe pattern. We suggest the former and do not emphasize the latter in explaining the emission for the same reason as discussed by *Kurth et al.* [2001]: The broadband bursts (0258:30–0259:30 SCET) consisting of very quickly drifting tones evolve into well-defined and distinct separate narrow tones with fast fluctuating center frequencies (0259:30–0259:45 SCET), and then stabilize finally into narrow tones with slowly updrifting center frequencies (>0259:45 SCET). The separate narrow tones with fast fluctuating center frequencies are not easily explainable by a diffraction processes and more easily explainable as a radial variation in the gradient position giving rise to a modest ECH frequency excursions (see Figure B3).

[35] While the emission itself is not considered a result of a fringe pattern, the density structure shown in Figure 4 might actually induce an interference effect on higher frequency emission like DAM. Specifically, *Imai et al.* [1997] examined the DAM modulation lanes near 23 MHz and determined that a density screen or grating out near Io's orbit must exist, with spacing between the density enhancement/depletions on the order of a few hundred kilometers. This derived spacing required for the observed DAM modulation lanes is on the same order as the high-frequency fingers remote-sensed by Cassini (i.e., Figure 4). Thus previous ground-based measurements of DAM may have also remote-sensed the extended finger structures associated with an interchange instability discussed herein.

[36] Finally, we demonstrate that the inversion of known radio emission models allows us to infer the characteristics

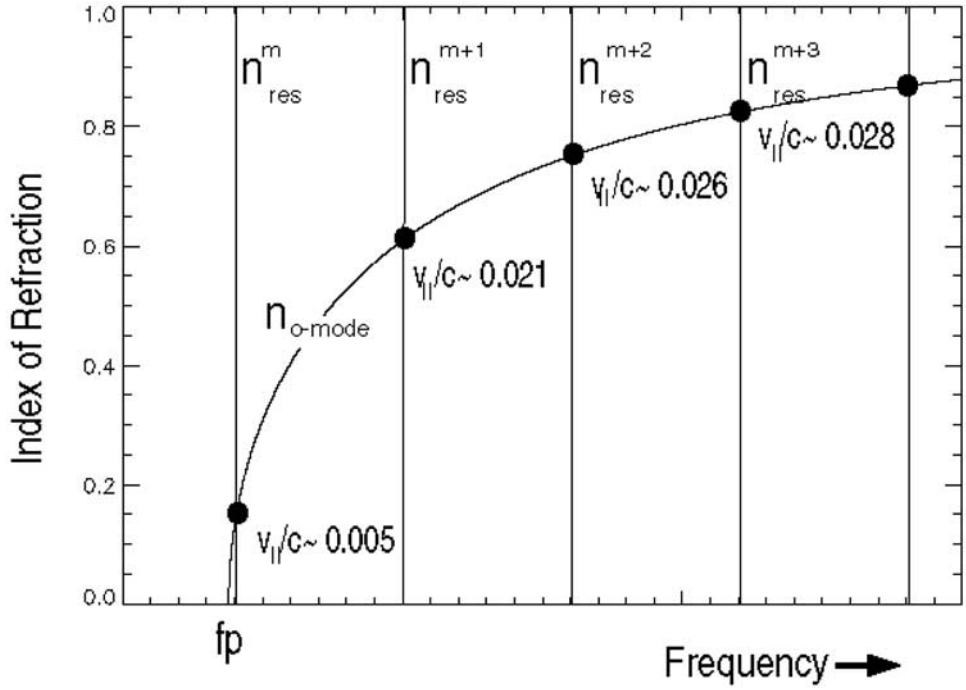

Figure A1. The interception of the ECH resonant indices of refractions with the o-mode branch. The resonant velocity is derived via equation (A5) for an 89° wave normal angle.

of the Io torus. Banded emissions indicate a torus with a sharp density boundary (like in Figure 2), and the tonal drifting is indicative of radial movement of this boundary. As we suggest, this movement can become quite vigorous generating broadband emissions from narrow interchange instability finger extensions. As discussed in Appendix C, monitoring the occurrence of Jovian kilometric bull's-eyes may indicate when the torus is undergoing a large-scale interchange instability like that envisioned by *Yang et al.* [1992, 1994], this driven by solar wind pressure pulses. In essence, kilometric emission from Jupiter is yielding clues on the conditions of the torus, and consistent monitoring of the emission may be a valuable tool in deconvolving the state of the inner Jovian magnetosphere.

Appendix A: Electron Cyclotron Harmonic (ECH) Resonance Condition

[37] *Jones* [1976] has suggested an electrostatic wave to electromagnetic o-mode wave coupling process for generating electromagnetic emissions near $f_{uh} \sim (n + 1/2)\, f_c$. Another possibility is that emissions are generated directly by anisotropic electron distributions in the region. A condition required for ECH wave/electron interaction is that the wave phase velocities v_p are comparable with the electron velocities in the phase space region where the anisotropy exists: $v_p \sim v_{electron}(df/dv_\perp > 0)$, where f is the electron velocity distribution function. We will demonstrate that v_p can attain small values and is capable of resonating with mildly energetic electrons.

[38] The complete electron cyclotron resonance condition with relativistic effects is

$$\omega - k_\parallel v_{\parallel res} = m\omega_c \gamma^{-1}, \tag{A1}$$

which can be reexpressed (with $\gamma^{-1} \sim (1 - v^2/2c^2)$) as

$$n^m_{res} = A(1 - Y_m(1 - B)), \tag{A2}$$

where $A = c/(v_\parallel \text{ Cos } \theta)$, $Y_m = mf_c/f$, $B = v^2/2c^2$. The variable θ is the wave normal angle and m is the order of the cyclotron harmonic. We have made a subtle change in notation from the main text: m now represents the harmonic number and n is the index of refraction.

[39] Figure A1 illustrates the resonance condition for $f > f_p \gg f_c$ defined by equation (A2). Note that for each n^m_{res}, a zero exists at $f = (1 - B)\, m\, f_c$, and the slope of the resonant index is $dn^m_{res}/df \sim mf_cA\,(1 - B)/f^2$. For large wave normal angles (consistent with the o-mode) and mildly energetic electrons ($v/c \sim 0.01$–0.1), the resonant index for each harmonic, n^m_{res}, has a very steep slope (almost vertical on an n vs f plot) with an origin near but very slightly downshifted from each mf_c. In essence, for very oblique wave normal angles and electron velocities below 10 keV, the curves appear generically like the steeped sloped versions presented in Figure A1. As $v_\parallel$ approaches zero, the slope of the index approaches infinity.

[40] Consider now the resonant index for the m-th ECH, n^m_{res}, and wave frequencies very near mf_c. Under these circumstances, $f \sim mf_c$, $Y_m \cong 1$ and $B = v^2_\parallel/2c^2 + v^2_\perp/2c^2$ making equation (A2) a most interesting form:

$$n^m_{res} = (2\text{Cos}\theta)^{-1}\left[(v_\parallel/c) + (v_\perp/v_\parallel)(v_\perp/c)\right]. \tag{A3}$$

Because the curve of n^m_{res} is very steep, much of the curve fits the condition that $Y_m \cong 1$, making equation (A3) applicable at most points along each of the curves in Figure A1. In essence, each of the curves in Figure A1 are so steep as to be nearly independent of frequency (i.e., for

each defined values of m, they exist essentially at a single frequency). As implied in Figure A1, resonance occurs between the waves and electrons at points where the resonance condition intercepts the mode: $n^{m}_{res} = n_{omode}$. These locations are indicated in the figure (i.e., thick dots). At these locations, equation (A3) is equal to the o-mode index of refraction, and we thus obtain:

$$(2\mathrm{Cos}\theta)^{-1}\left[(v_{\|}/c) + (v_{\perp}/v_{\|})(v_{\perp}/c)\right] = (1 - X)^{1/2}, \qquad (A4)$$

where $n_{omode} = (1 - X)^{1/2}$ and $X = f_p^2/f^2$. For a case of $v_{\|} > v_{\perp}$, we can derive an approximate expression for the parallel resonant electron velocity for each ECH at locations where $n^{mo}_{res} = n_{omode}$:

$$v_{\|res} \sim 2c\ \mathrm{Cos}\theta(1 - X)^{1/2}. \qquad (A5)$$

These resonant velocity values for an 89° normal angle are indicated at the intercept points in Figure A1. Note that the resonant velocity steadily increases with increasing ECH number above fp. Conversely, the resonant velocity becomes small as $f \sim mf_c$ approaches f_p. Thus those ECHs closest to f_p will have relatively modest wave phase velocities and thus be capable of resonating with any anisotropic low-energy electron distributions in the region. In fact, such distributions exist at plasma density gradients like the plasmapause [*Kurth et al.*, 1979] and are responsible for the electrostatic $(n + 1/2)f_c$ emissions. These same distributions would then radiate ECH emissions at harmonic frequencies just above the o-mode cutoff (e.g., Figure 3).

[41] Figure A1 shows the emissions at one value of f_p. Near a density gradient, the o-mode curve in Figure A1 slides upward (for increasing density), passing by successive harmonics. In the processes the resonance velocity for each harmonic will also steadily decrease as fp approaches and passes over the m + 1, m + 2, etc., harmonic. Consequently, along a plasma gradient each of the harmonics can be excited as f_p approaches mf_c, $(m + 1)f_c$, etc., giving rise to a set of narrowband tones like that illustrated in Figure 2.

[42] It is thus evident that moderately energetic electrons can indeed directly interact with o-mode waves near the local plasma frequency via the relativistic electron cyclotron harmonic resonance. Equation (A5) can only be realized by including the relativistic terms in the resonance condition. Without relativistic terms, the velocity dependence on $(1 - X)^{1/2}$ is inverse rather than direct.

[43] One theoretical note: equation (A5) describing the parallel resonance velocity can be compared with the full-form resonant velocity condition defined in equation (15) in the work of *Farrell* [2001]. In its full form, the resonant velocity forms an ellipse in phase space with ellipse center, v_c, lying on the $v_{\|}$ axis with ellipse intercepts at $v_c + v_{ma}$ and $v_c - v_{ma}$, v_{ma} being the ellipse semimajor axis. The variable $v_c = B/A$ and $v_{ma} = D/Y_m$, where $A = (Y_m^2 + n^2\mathrm{Cos}\theta^2)^{1/2}$, $B = cn\mathrm{Cos}\theta/A$, and $D = (c^2(Y_m^2 - 1) + B^2)^{1/2}$. For $Y_m \sim 1$ and $n\mathrm{Cos}\theta \ll 1$, it is easy to demonstrate that $v_c \sim v_{ma} \sim cn\mathrm{Cos}\theta \sim c\mathrm{Cos}\theta(1 - X)^{1/2}$. Consequently, the value of equation (A5) is comparable to being located at the ellipse/$v_{\|}$ axis intercept at $v_c + v_{ma}$, at the ellipse's most energetic parallel point. As such, equation (A5) above represents the upper bound to the possible parallel velocities and represents a good indicator for the ellipse location in phase space, particularly near the $v_{\|}$ axis.

Appendix B: Evolution of ECH structure from Narrowband to Broadband Emission

[44] As evident in Figure 1, broadband emissions observed from 0258:30 to 0259:30 SCET evolved into a set of discrete tones possessing oscillations in frequency between 0259:30 and 0300:00 SCET. These oscillations made the tones appear broadened in bandwidth (although not completely broadbanded as before 0259:30 SCET). Finally, the oscillating bands became stable forming distinct narrow tones that slowly up-drifted in frequency over the minute between 0300:00 and 0301:00 SCET.

[45] We present a source emission model that assumes the radiation originates from a distinct plasma gradient generating narrow ECH-related emissions and that the emission variation results from the changing position of the gradient in the Jovian magnetosphere. The gradient is assumed to be positioned at the outer edge of the Io torus, between 8 and 10 R_J. To replicate the emission frequency-time pattern, we assume an r/φ position for the gradient and assume a direct ray of harmonic emission from the source to a distant observer.

[46] For the gradient position $\nabla n(r, \varphi)$, we assume a radial gradient positional variation of the form

$$r = r_o + A_1(\varphi)\sin(2\pi N_1\Delta\varphi/\varphi_{tot}) + A_2(\varphi)\sin(2\pi N_2\Delta\varphi/\varphi_{tot}), \qquad (B1)$$

where r_o is the gradient radial location at simulation start longitude ($\varphi = 0$). There are two sine-function terms to represent (1) large-scale and (2) small-scale oscillations in the gradient location. The variable A_1 is the amplitude of an assumed large-scale radial variation in the gradient location and N_1 is the number of gradient radial oscillation across the simulation box, with the value being small (~1). The variable A_2 is the amplitude of small-scale gradient fluctuations and N_2 is the number of associated cycles (numerous). The box size is φ_{tot} in azimuthal width, representing about 1°.

[47] Figures B1–B3 shows the resulting pattern for (a) slow drifting gradient position, (b) fast changing gradient position, and (c) a case resembling that in Figure 1b. Figures B1 and B2 are for demonstration purposed, and Figure B2 is representative (but not an exact replica) of Figure 1b. Figure B1 has $r_o = 11.0$, $A_1 = -2.0$, $N_1 = 0.25$ (gradient location variation over 1/4-cycle) and $A_2 = 0$ (no small-scale structures). Note that as the gradient slowly drifts to progressively lower radial positions, the cyclotron harmonics up-drift, much like the up-drift observed between 0300:00 and 0301:00 SCET. Figure B2 shows the effect of a small scale gradient variation, with the model run at $r_o = 10.$, $A_1 = 0$ and $A_2 = 3\exp(-\gamma\ \mathrm{abs}(\varphi - \varphi_o))$ with γ a decaying factor of the quick oscillations in azimuth and φ_o a displacement in azimuth (to center the pulse-shaped displacement in the figure). The variable N_2 is set to 50. Note that a quick change in radial position in the gradient gives rise to a broadband emission, with the harmonics

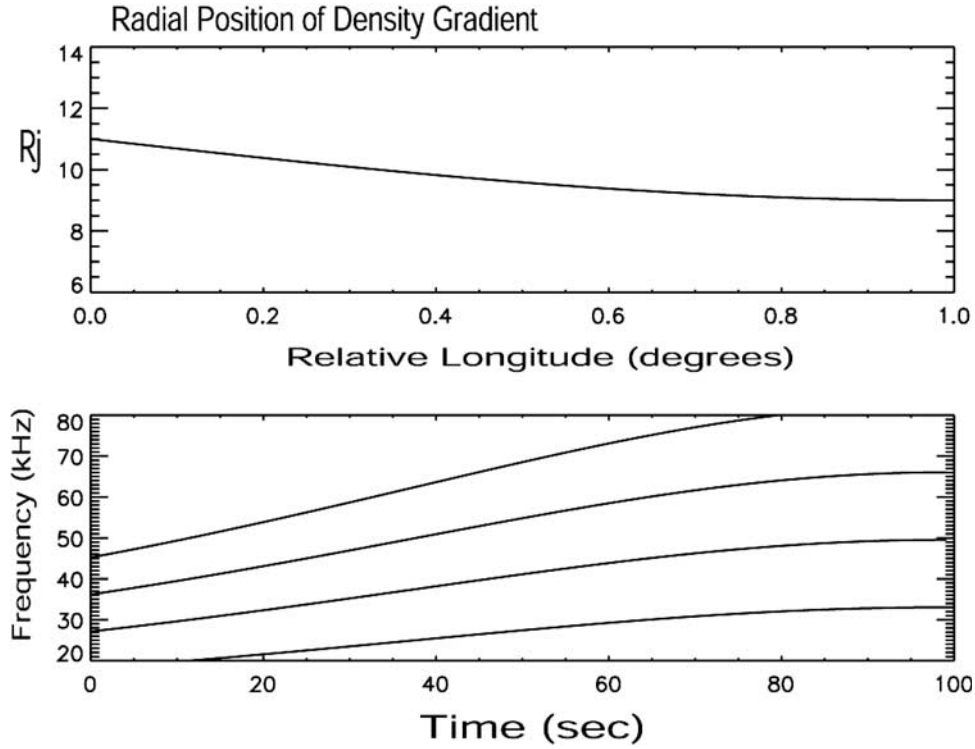

Figure B1. A model showing the slowly changing gradient location and the associated slow updrift of the cyclotron harmonic-related emissions.

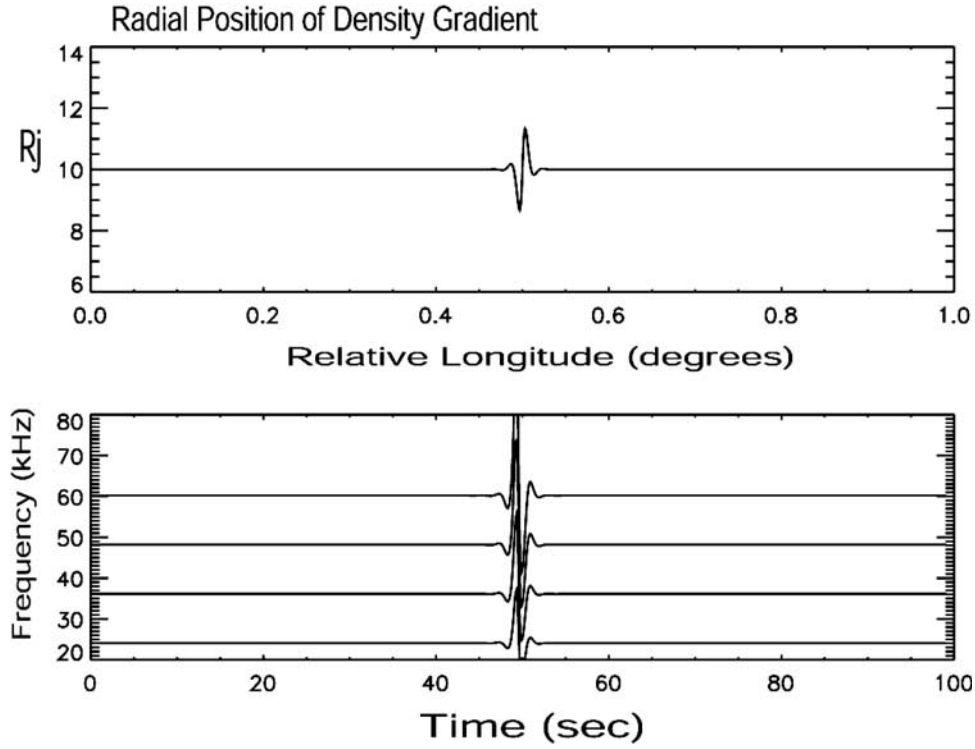

Figure B2. A model showing a quick change in gradient location and the associated development of a broadband emission (merged or ''smeared'' narrow tones) due to the fast change in cyclotron harmonic frequency in a spatially localized region.

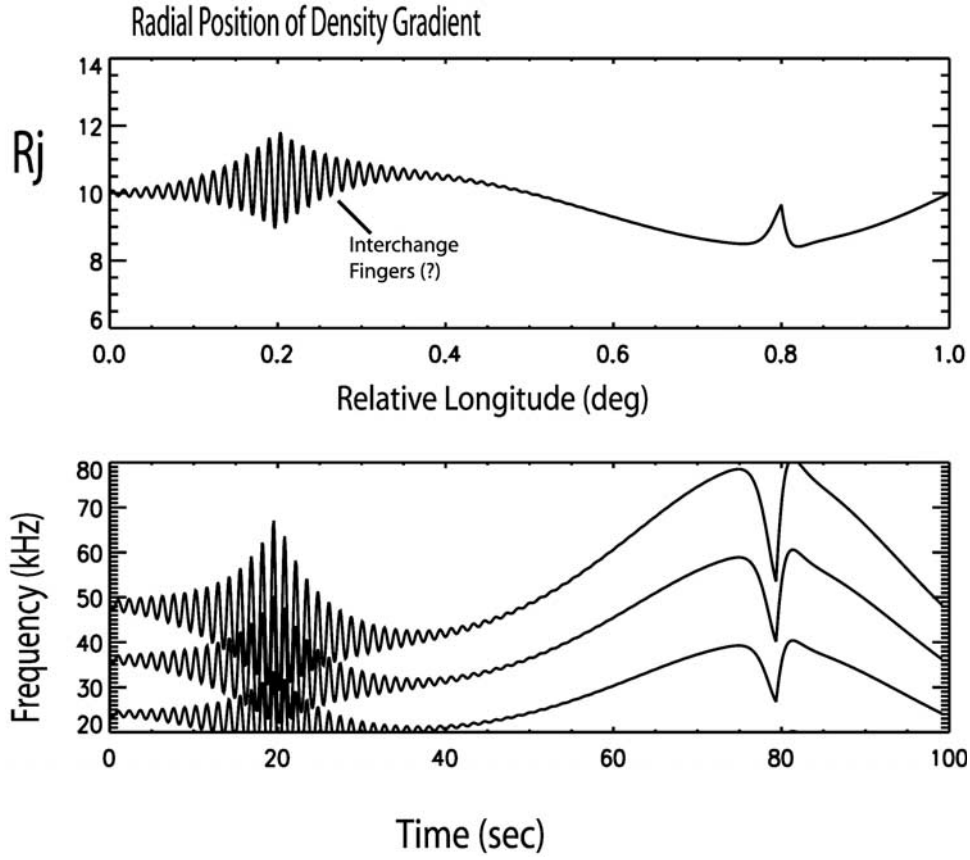

Figure B3. A simplified model of the activity in Figure 1b, including a long-period oscillation, a set of fast finger-like wave structures (possibly associated with an interchange instability on the convex portion of the surface) and a third, single density jetty in the bubble center (placed in model near 0.8 degrees).

sweeping a large frequency extent in a short period of time in association with the gradient's radial position. Such events are like those observed between 0258:30 and 0259:30 SCET.

[48] Figure B3 shows a representative portion of Figure 1, with $r_o = 10.0$, $A_1 = 2\varphi$, $A_2 = 1.5\exp(-\gamma\ \mathrm{abs}(\varphi - \varphi_o))$, $N_1 = 1.0$, and $N_2 = 75$. In order to further model the gradient position, a third variation, an enhancement found in the center of the bubble, was included by adding an isolated density jetty described by $A_j(\varphi)\ \sin\ (2\pi\ N_\varphi \Delta\varphi/\varphi_{tot})$ with $A_j = 2\exp(-\gamma_j\ \mathrm{abs}(\varphi - \varphi_{oj}))$ term. The damping coefficient, γ_j, is very large to create an isolated 1/2-wavelength structure (an outward-directed density jetty). In Figure 3, the large-scale density bite-out is recreated along with high-frequency finger-like density structures superimposed along the convex portion of the primary bite-out. The variable φ_o is set to zero, giving the largest small-scale fluctuation near $\varphi = 0^\circ$. Figure B3a shows the density structure and Figure B3b shows the cyclotron harmonic signature. We modeled the small-scale density fingers to exponentially-decay as they enter the concave portion of the gradient location. As suggested by Figure 1b, this density model results in cyclotron harmonic emission that transforms from merging narrow tones (forming periodically spaced broad-band bursts) into a set of narrow tones with quickly varying center frequencies that finally stabilize into the set of slow-drifting narrow tones seen in the concave portion of the biteout.

Appendix C: An Explanation of Jovian Bull's-Eyes

[49] *Kaiser and MacDowall* [1998] found that Jovian VLF radiation could appear, on special occasions, as a set of nested U-shaped narrow tones forming a "bull's-eye" pattern on a Ulysses URAP low-band radio spectrogram (see Figure C1). These events often lasted for a few hours. Sets of these events (sometime four or five in a row spaced a couple of hours apart) were found to occur for about 2 days immediately following a large solar wind ram pressure increase (a "pressure pulses") on the Jovian frontside magnetosphere. The solar wind pressure/bull's-eye occurrence was monitored for over 6 months during Ulysses 1991–1992 approach to Jupiter and the correlation between the two was found to be extraordinarily strong [see *Kaiser and MacDowall*, 1998, Figure 3].

[50] By analogy to the explanation for the Cassini event in Figure 1, we may now have a possible explanation for these unusual kilometric bull's-eye structures observed by Ulysses. Specifically, during the solar wind ram pressure increase, the Jovian frontside magnetosphere compresses. The increasing magnetic pressure on the frontside region

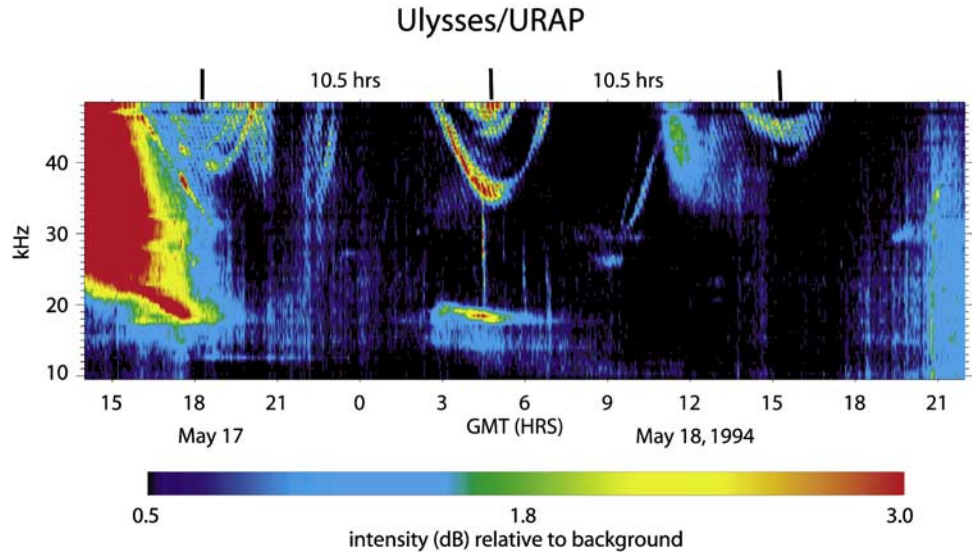

Figure C1. A Ulysses spectrogram adapted from *Kaiser and MacDowall* [1998] which shows a sequence of Jovian bull's-eye emissions, appearing as a set of nested U-shaped arcs, at 0600 GMT and 0900 GMT and 1600 GMT. These emissions tended to appear for a few days immediately following the incidence of large solar wind pressure pulses [*Kaiser and MacDowall*, 1998].

pushes inward on the torus and increases the torus' stability to the interchange mode. However, once the solar wind pressure pulse passes by Jupiter, the magnetopause quickly expands outward, almost-impulsively releasing the pressure on the frontside torus. We suspect that the torus then becomes unstable to the interchange process during this rarefaction period, and forms radially extended, well-defined density fingers similar to (but slightly larger than) that presented in the MHD simulation of *Yang et al.* [1992, 1994].

[51] ECH emission from such interchange-related density gradient extensions can account for the nested narrowband tones that form the U-shaped emission. Figure C2 shows the ECH emission from a set of model radially extended fingers

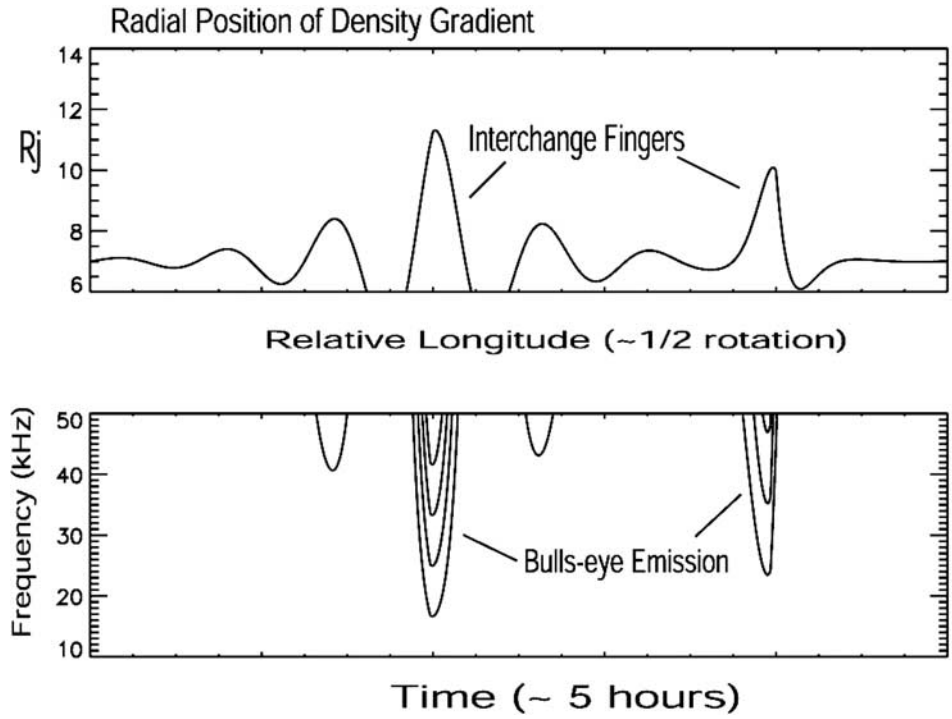

Figure C2. The ECH emission model of simulated torus density gradients presumed to be formed via the large-scale interchange instability described by *Yang et al.* [1992, 1994]. Note that ECH emission from such structures gives rise to the "bull's-eye" appearing torus kilometric emission.

that approximate the *Yang* [1992, 1994] fingers (using the model in Appendix B). Note that as these structures corotate past a distant observation point, the density gradient position extends outward, corresponding to ECH emission with decreasing frequency tones. As the gradient position extends inward again, the ECH emissions drift upward. The results of the outward-then-inward gradient position resulted in the U-shaped bull's-eye emission.

[52] In this interpretation, each individual bull's-eye indicates the passage of a single large interchange instability density finger similar to that modeled by *Yang et al.* [1992, 1994]. The U-event duration indicates the longitudinal width of the density finger and the frequency excursion indicates the radial displacement. From the figures presented in the work of *Kaiser and MacDowall* [1998], the longitude width of the fingers is $\sim 100^\circ$ and their radial extension is $1-3\ R_J$ to account for the observed frequency drifts. Finally, the number of bull's-eyes indicates how many density fingers are present on the torus surface (anywhere from 1 to 6) [*Kaiser and MacDowall*, 1998]. The interchange instability operates no more than a few days immediate following the solar wind ram increase (i.e., initiated during magnetospheric rarefaction), after which, pressure balance is reestablished on the torus frontside. The finger structures and associated bull's-eye events disappear until another solar wind pressure pulse again compresses the inner magnetosphere.

[53] **Acknowledgment.** Arthur Richmond thanks Stuart D. Bale and Helmut O. Rucker for their assistance in evaluating this paper.

References

Acuna, M. H., K. W. Behannon, and J. E. P. Connerney (1983), Jupiter's magnetic field and magnetosphere, in *Physics of the Jovian Magnetosphere*, edited by A. J. Dessler, Cambridge Univ. Press, New York.

Aggson, T. L., et al. (1993), Equatorial electric field observations, *Adv. Space Res.*, *13*, 271.

Bagenal, F. (1994), Empirical model of the Io torus: Voyager measurements, *J. Geophys. Res.*, *99*, 11,043.

Barbosa, D. D. (1981), Fermi-Compton scattering due to magnetopause surface fluctuations in Jupiter's magnetospheric cavity, *Astrophys. J.*, *243*, 1076.

Basu, S., et al. (1986), Gigahertz scintillations and spaced receiver drift measurements during project Condor equatorial spread-F region rocket campaign in Peru, *J. Geophys. Res.*, *91*, 5526.

Carr, T. D., M. D. Desch, and A. K. Alexander (1983), Phenomenology of the magnetospheric radio emissions, in *Physics of the Jovian Magnetosphere*, edited by A. J. Dessler, Cambridge Univ. Press, New York.

Desch, M. D., W. M. Farrell, and M. L. Kaiser (1994), Asymmetries in the Io plasma torus, *J. Geophys. Res.*, *99*, 17,205.

Farrell, W. M. (2001), Direct generation of o-mode emission in a dense, warm plasma: Applications to interplanetary type II emissions and others in its class, *J. Geophys. Res.*, *106*, 15,701.

Farrell, W. M., R. J. MacDowall, R. A. Hess, M. L. Kaiser, M. D. Desch, and R. G. Stone (1993), An interpretation of the broadband VLF waves near the Io torus as observed by Ulysses, *J. Geophys. Res.*, *98*, 21,177.

Farrell, W. M., R. A. Hess, and R. J. MacDowall (1999), O-mode emission at the Io torus: A real or virtual source, *Geophys. Res. Lett.*, *26*, 1.

Green, J. L., and D. A. Gurnett (1980), Ray tracing of Jovian kilometric radiation, *Geophys. Res. Lett.*, *7*, 65.

Green, J. L., et al. (2002), On the origin of kilometric continuum, *J. Geophys. Res.*, *107*(A7), 1105, doi:10.1029/2001JA000193.

Gurnett, D. A. (1975), The Earth as a radio source: The nonthermal continuum radiation, *J. Geophys. Res.*, *80*, 2751.

Gurnett, D. A., W. S. Kurth, and F. L. Scarf (1983), Narrowband electromagnetic emissions from Jupiter's magnetosphere, *Nature*, *302*, 385.

Gurnett, D. A., et al. (2002), Control of Jupiter's radio emission and aurorae by the solar wind, *Nature*, *415*, 985.

Gurnett, D. A., et al. (2004), The Cassini radio and plasma wave investigation, *Space Sci. Rev*, in press.

Imai, K., L. Wang, and T. D. Carr (1997), Modeling Jupiter's decametric modulation lanes, *J. Geophys. Res.*, *102*, 7127.

Jones, D. (1976), Source of terrestrial nonthermal radiation, *Nature*, *260*, 686.

Jones, D. (1986), Io plasma torus and the source of Jovian kilometric radiation (bKOM), *Nature*, *324*, 40.

Jones, D., and Y. Leblanc (1987), Source of broad-band Jovian kilometric radiation, *Ann. Geophys. A*, *5*, 29.

Kaiser, M. L. (1998), Jovian and terrestrial low-frequency radio bursts: Possible causes of anomalous continuum, *J. Geophys. Res.*, *103*, 19,993.

Kaiser, M. L., and R. J. MacDowall (1998), Jovian radio "bullseyes" observed by Ulysses, *Geophys. Res. Lett.*, *25*, 3113.

Kaiser, M. L., et al. (1992), Ulysses observations of escaping VLF emissions from Jupiter, *Geophys. Res. Lett.*, *17*, 649.

Kelley, M. C., et al. (1986), The Condor equatorial spread-F campaign: Overview and results of large-scale measurements, *J. Geophys. Res.*, *91*, 5487.

Kurth, W. S., et al. (1979), A comparison of intense electrostatic waves near f_{uhr} with linear instability theory, *Geophys. Res. Lett.*, *6*, 487.

Kurth, W. S., D. A. Gurnett, and F. L. Scarf (1980), Spatial and temporal studies of Jovian kilometric radiation, *Geophys. Res. Lett.*, *7*, 61.

Kurth, W. S., D. A. Gurnett, and R. R. Anderson (1981), Escaping nonthermal continuum radiation, *J. Geophys. Res.*, *86*, 5519.

Kurth, W. S., D. A. Gurnett, S. J. Bolton, A. Roux, and S. M. Levin (1997), Jovian radio emissions: An early overview of Galileo observations, in *Planetary Radio Emissions IV*, edited by H. O. Rucker, S. J. Bauer, and A. Lecacheux, Austrian Acad. of Sci. Press, Vienna.

Kurth, W. S., et al. (2001), High resolution observations of low frequency Jovian radio emissions by Cassini, in *Planetary Radio Emissions V*, edited by H. O. Rucker et al., Austrian Acad. of Sci. Press, Vienna.

Kurth, W. S., et al. (2002), The dusk flank of Jupiter's magnetosphere, *Nature*, *415*, 991.

LaBelle, J., and M. C. Kelley (1986), The generation of kilometer scale irregularities in equatorial spread-F, *J. Geophys. Res.*, *91*, 5504.

Ladreiter, H. P., P. Zarka, and A. Lecacheux (1994), Direction finding study of Jovian hectometric and broadband kilometric radio emissions: Evidence for their auroral origin, *Planet. Space Sci.*, *42*, 919.

Omidi, N., C. S. Wu, and D. A. Gurnett (1984), Generation of auroral kilometric and z-mode radiation by the cyclotron maser mechanism, *J. Geophys. Res.*, *89*, 883.

Stone, R. G., et al. (1992), Ulysses radio and plasma wave observations in the Jupiter environment, *Science*, *257*, 1524.

Tidman, D. A., and N. A. Krall (1971), *Shock Waves in Collisionless Plasmas*, John Wiley, New York.

Warwick, J. W., et al. (1979), Voyager 1 planetary radio astronomy observations near Jupiter, *Science*, *204*, 995.

Wu, C. S., and L. C. Lee (1979), A theory for terrestrial kilometric radiation, *Astrophys. J.*, *230*, 621.

Yang, Y. S., et al. (1992), Numerical simulation of plasma transport driven by the Io torus, *Geophys. Res. Lett.*, *19*, 957.

Yang, Y. S., et al. (1994), Numerical simulation of torus-driven plasma transport in the Jovian magnetosphere, *J. Geophys. Res.*, *99*, 8755.

Zalesak, S. T., S. L. Ossakow, and P. K. Chaturvedi (1982), Nonlinear equatorial spread-F: The effect of neutral winds and background Pedersen conductivity, *J. Geophys. Res.*, *87*, 151.

M. D. Desch, W. M. Farrell, M. L. Kaiser, and R. J. MacDowall, NASA Goddard Space Flight Center, Greenbelt, MD 20771, USA. (michael.desch@gsfc.nasa.gov; william.farrell@gsfc.nasa.gov; michael.l.kaiser@gsfc.nasa.gov; robert.macdowall@gsfc.nasa.gov)

D. A. Gurnett, G. B. Hospodarsky, and W. S. Kurth, Department of Physics and Astronomy, University of Iowa, Iowa City, IA 52240, USA. (donald-gurnett@uiowa.edu; gbh@space.physics.uiowa.edu; william-kurth@uiowa.edu)